Bi-directional LEEM and eV-TEM spectroscopy on a graphene-hBN heterostack

Neu, P.S.; Krasovskii, E.E.; Tromp, R.M.; Molen, S.J. van der

Ultramicroscopy 271 (2025) 114117

Contents lists available at ScienceDirect

Ultramicroscopy

journal homepage: www.elsevier.com/locate/ultramic

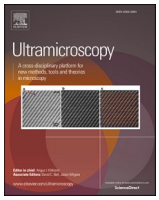

Bi-directional LEEM and eV-TEM spectroscopy on a graphene-hBN heterostack

Peter S. Neu [a,*], Eugene E. Krasovskii [b,c,d], Rudolf M. Tromp [e,a], Sense Jan van der Molen [a]

[a] Universiteit Leiden, Institute of Physics, Niels Bohrweg 2, Leiden, NL 2333 CA, Netherlands
[b] Universidad del Pais Vasco, Apartado de Correos 1072, San Sebastián/Donostia, País Vasco, ES 20080, Spain
[c] Basque Foundation for Science, Plaza Euskadi 5, Bilbao, Bizkaia, ES 48009, Spain
[d] Donostia International Physics Center, Paseo Manuel de Lardizabal, 4, San Sebastian, País Vasco, ES 20018, Spain
[e] IBM Research, T.J. Watson Research Center, P.O. Box 218, Yorktown Heights, NY 10598, USA

ARTICLE INFO

Keywords:
LEEM
eV-TEM
Unoccupied states
Probing depth
Interference
Van der Waals

ABSTRACT

Van der Waals heterostacks can exhibit emergent properties as a result of the coupling between the individual layers stacked. Here we focus on heterostacks of graphene and hBN, and study both coherent electron resonances (or unoccupied states) and inelastic losses. For this, we measure electron reflection and transmission spectra of the stack, as a function of electron energy. Special attention is paid to the symmetry upon flipping the heterostack, i.e., whether the electrons are first incident on the graphene or on the hBN surface: whereas electron reflection may be sensitive to sample orientation, electron transmission should not. Experimentally, we compare LEEM (reflection) and eV-TEM (transmission) IV spectra measured on free-standing graphene-hBN heterostacks with either the graphene or hBN side facing the LEEM objective lens. Resonances and inelastic loss are first modeled with the help of a simple wave interference toy model inspired by optics. More advanced calculations are performed to obtain the spatially resolved density of unoccupied states in the heterostack. We relate these calculations to the measured spectra, taking into account the finite probing depth of the reflected electron beam.

1. Introduction

Stacking two different van der Waals (vdW) materials produces a heterostructure that breaks the out-of-plane symmetry of a sample [1]. The graphene-hBN heterostack specifically is commonly used in experiments, where hexagonal boron nitride (hBN) provides an insulating flat surface for graphene with a minimal lattice mismatch [2,3]. Placing graphene on or between hBN is known to yield better transport characteristics (e.g., higher charge carrier mobility in graphene [4–6] than on other common substrates like silicon and silicon nitride. Furthermore, it is in hBN sandwich structures that superconductivity in twisted bilayer graphene is found [7]). It is generally assumed that the coupling of hBN to the graphene can be neglected at the Fermi level, as hBN is a large band gap insulator [8,9].

Like graphene, hBN is a vdW material with a hexagonal lattice, with all boron (B) and nitrogen (N) atoms located in one plane. Following a wave interference toy model [10], one can expect interlayer states (i.e. unoccupied electronic states located between atomic layers) in multilayer hBN just like in multilayer graphene [11,12], and even in a graphene-hBN heterostack. These states should be observable in LEEM IV-spectroscopy, provided they are above the vacuum energy.

Indeed, Hibino et al. [13] have previously reported on mono- and bilayer graphene on top of mono- and bilayer hBN on a cobalt (Co) surface. Their LEEM-IV spectra show a characteristic interlayer state minimum even for one-layer graphene on one-layer hBN, and a splitting of the minimum upon adding more layers of graphene and/or hBN.

Jobst et al. [14] have also investigated hBN interlayer states using LEEM. They observed a splitting of the hBN interlayer states for two to five layers of hBN on silicon, similar to the case of two to five layers of graphene. Furthermore, they presented self-consistent electronic structure calculations showing that few-layer graphene on *bulk* hBN retains its characteristic splitting of the interlayer state, while few-layer graphene on few-layer hBN should show a mixed interlayer state.

In this work, we present and discuss measurements on freestanding hBN-on-graphene heterostructures, thus removing the substrate from the system. For this, our multilayers are suspended over the 2-μm holes

* Corresponding author.
E-mail address: neu@physics.leidenuniv.nl (P.S. Neu).

https://doi.org/10.1016/j.ultramic.2025.114117
Received 17 September 2024; Received in revised form 21 January 2025; Accepted 15 February 2025
Available online 16 February 2025

of a TEM grid. We present LEEM- and eV-TEM IV spectra of these free-standing heterostructures and compare these to the previously published reports. The fact that the sample is prepared on a TEM grid also allows us to investigate the role of symmetry: We can flip the sample and measure LEEM and eV-TEM spectra on the reversed order of layers. We model our system in two ways. Initially, we apply a simple toy model to get an intuition for the problem. Subsequently, we compare the experimental data to calculations of reflection and transmission obtained by constructing the Bloch eigenfunctions of the different graphene-hBN heterostacks.

2. Experiment

The sample was prepared from CVD-grown hBN and graphene (acquired from [15] and [16], respectively), transferred to a holey TEM grid (silicon nitride [17]). First, the holey TEM grid was sputter-coated with 5 nm platinum/palladium from both sides to make it conductive and thus prevent charging by absorbed electrons. Next, we float a glass frame on a 0.1 M ammonium persulfate (APS) solution and place the CVD-grown graphene on Cu inside the frame. Following the polymer-free transfer method [18], the surface tension of the etchant prevents the graphene from crumbling onto itself. Once the Cu is removed, the graphene is picked up by lowering the hBN on Cu onto it. Then the stack is flipped, such that the Cu is on the bottom, and the process is repeated to etch away the copper. Finally, the floating graphene on hBN is picked up from the top with the sputter-coated SiN TEM grid. The resulting stack on the TEM grid is tilted away to break the surface tension and the excess etchant left on the surface is blotted away with filter paper. We note that no additional cleaning steps have been performed, i.e., the graphene and hBN surfaces in contact with each other have been exposed to air and the outer surfaces of the stack were in contact with Cu and etchant.

Two free-standing areas of the sample are shown in Fig. 1, with the micrographs recorded both in LEEM (Fig. 1a,c) and eV-TEM (Fig. 1b, d) mode. In the usual orientation of the TEM grid, i.e., with the flat side towards the LEEM objective lens, the resulting order of layers as seen from the LEEM objective lens-side is: hBN (on top of) / graphene (on top of a holey) / SiN TEM grid. A comparison to a previous LEEM inspection of the individual CVD-grown materials - still on their copper substrates - indicates that the multilayer areas of elongated tears (Fig. 1, blue arrows) or folds are in the graphene and the triangular multilayer areas (Fig. 1, red and yellow arrows) are in the hBN.

The graphene/hBN film on the TEM grid (Fig. 1) does not show tears, indicating that the majority of the sample is covered by a monolayer of graphene with a monolayer of hBN on top, denoted as 1Gr1hBN. The other layer combinations are enumerated by their graphene (Gr) and hBN count, inferred from the shapes of the features. Below, we will confirm the layer count by comparing the spectra measured to the previous publication of Hibino et al. [13].

The option of flipping the sample allows us to acquire four spectra per heterostructure and compare these to the considerations about symmetry. These four spectra cover all possibilities of perpendicular electron transmission and reflection of the sample. In the left column of Fig. 2, we show spectra recorded in the usual configuration (with the

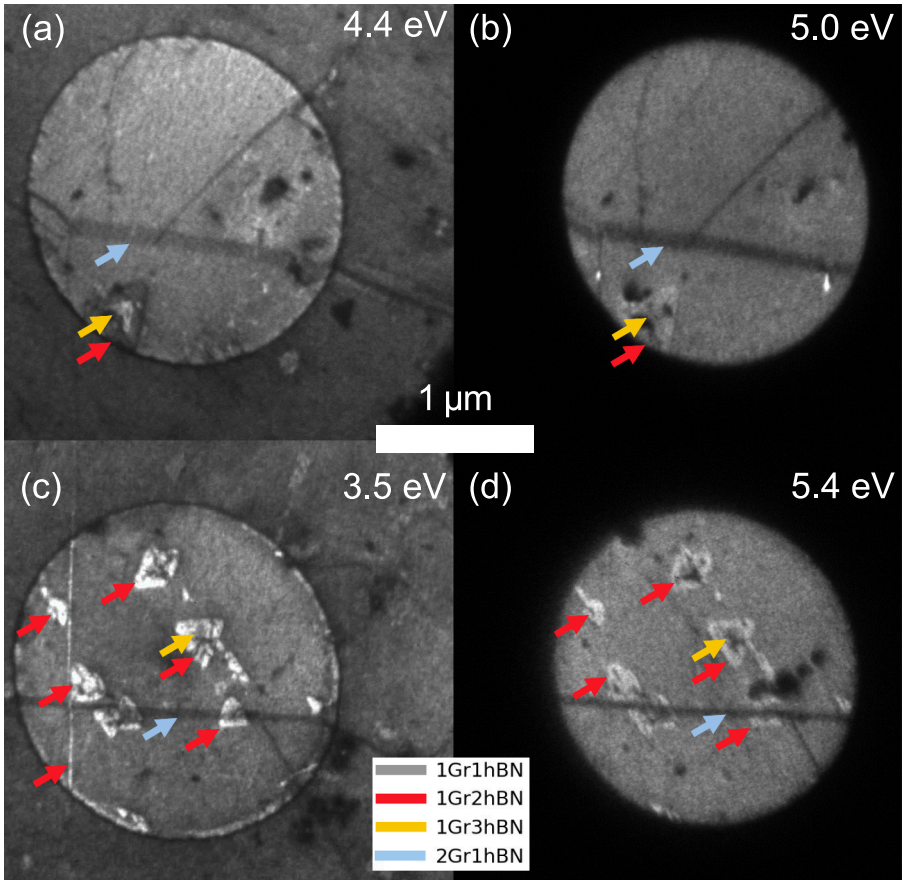

Fig. 1. LEEM images (a,c) and eV-TEM images (b,d) of the hBN-on-graphene heterostack. While most areas are covered with one layer of hBN on top of one layer of graphene, some triangles of additional layers of hBN and lines of additional graphene layers show. The Pt/Pd-coated SiN support grid is impenetrable for the electrons and corrugates the layered material on top of it, compared to the free-standing areas. The arrows point to areas with an additional layer of graphene (2Gr1hBN) and additional layers of hBN (1Gr2hBN and 1Gr3hBN). The other areas are one layer of hBN on one layer of graphene (1Gr1hBN, not marked with arrows).

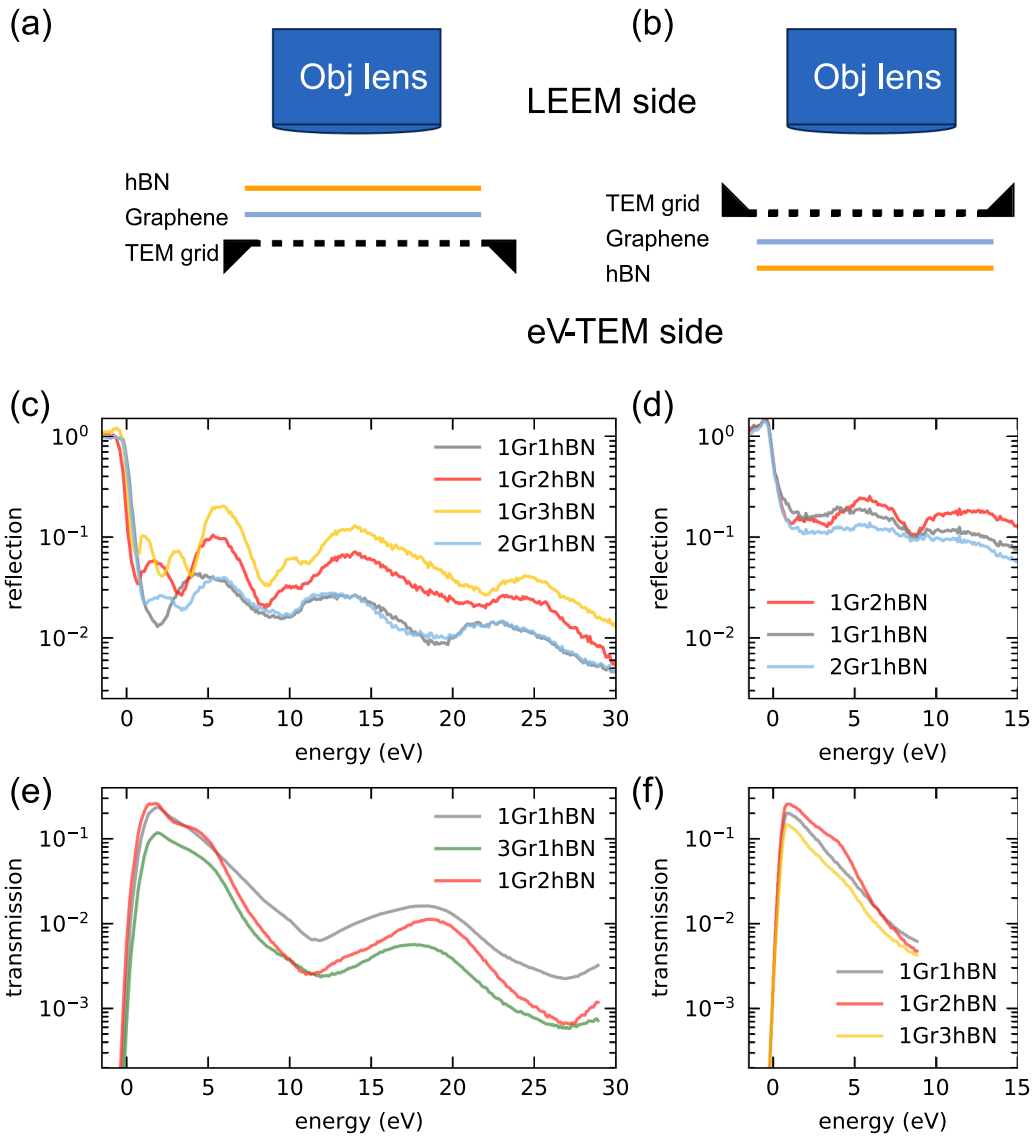

Fig. 2. Sketch of the graphene-hBN heterostack sample with (a) the original orientation (reflection from the hBN side), with the reflection spectra (c) and transmission spectra (e) measured in this configuration. For the subsequent measurements the sample was flipped as shown in (b) (reflection from the graphene side) and the reflection/transmission spectra (d) and (f), respectively, were acquired in this flipped orientation.

hBN side towards the LEEM lens as sketched in Fig. 2a), with the reflection spectra in Fig. 2c) and the transmission spectra in Fig. 2e). In the right column of Fig. 2, the spectra recorded in the flipped configuration (with the graphene side towards the LEEM lens as sketched in panel b) are depicted, with reflection and transmission spectra in panel 2d) and 2f), respectively.

The spectra d) and f), acquired with the flipped geometry, are cut off at 15 and 10 eV, respectively, as the spatial resolution, especially limited by astigmatism, does not allow for distinguishing between the areas of different layer count at higher energies. The imaging conditions are inherently worse in the flipped condition, as the holey silicon nitride (SiN) membrane is recessed ~300 μm into the SiN frame. Since the potential difference from the sample to the electron lens is much larger on the LEEM side (15 kV) than on the eV-TEM side (~200 V), the electric equipotential surfaces close to the TEM grid are much more curved, when the recessed - instead of the flat side – of the TEM-grid is facing the LEEM side. The in-plane electric field resulting from the curved equipotential planes deflects the electrons when imaging an area that is not at the center of the TEM grid. The deflection can be compensated to some degree by tilting the sample (relative to the LEEM lens), adjusting the centering on the aberration-correcting mirror, and – only in the LEEM case – adjusting the incidence angle of the electrons. However, we find that these compensations are optimal at a low energy and get worse with increasing energy.

The spectra in Fig. 2 show features that resemble interlayer resonances seen in multilayer graphene, as well as features that are unique to hBN spectra. The number of reflection minima associated with interlayer states (around 2.5 eV above vacuum level) only depends on the number of layers, not whether these are graphene or hBN layers. Like in freestanding graphene, there are $n-1$ minima for n layers. Before discussing the individual features, we will gain intuition for the expected interlayer resonances with the help of a simple interference toy model. After returning to the experimental spectra, we will relate their hBN-specific features to the density of states (above the vacuum level) calculated from first principles for different graphene/hBN stacks and different orientations.

3. Symmetry and inelastic toy model

In contrast to the multilayer graphene samples previously studied in

eV-TEM [10,19], the present hBN-on-graphene heterostacks clearly break the out-of-plane symmetry. We will first discuss what symmetries of the reflection/transmission coefficients to expect upon flipping the sample. Flipping the sample is equivalent to illuminating the sample with electrons from the opposite side.

In the case of fully elastic scattering the transmitted and reflected electron flux must be independent of the orientation, as implied by scatter matrix theory [20,21]. Hence, in the absence of inelastic scattering, we expect that the real-valued transmissivity T and reflectivity R of electrons remain the same for the flipped sample.

In practice, we will have to consider inelastic scattering as well. In that case, an asymmetric sample with a thickness larger than or comparable to the Mean Free Path (MFP) will not show the same reflectivity on both sides. To give a simple example: consider a silicon chip with a typical thickness of ~1 mm with graphene deposited on one side. On the graphene side, we expect to measure a graphene signal in LEEM, whilst only a Si signal is expected from the other side. The transmission for both cases, however, should be the same in general.

To investigate the role of elastic and inelastic scattering in the heterostack we first turn to a semiclassical wave interference toy model borrowed from thin film optics. For purely elastic scattering, at each graphene- or hBN-layer, the electron wave is partially reflected and partially transmitted with real-valued coefficients r and t, respectively, such that $r^2 + t^2 = 1$. To denote inelastic effects, we assume that the electron wave function amplitude is diminished by a real factor β at every layer (replacing r by $\beta{\cdot}r$, and t by $\beta{\cdot}t$, with $0 < \beta < 1$), corresponding to an inelastic scattering probability of $1 - \beta^2$ for every interlayer distance travelled. In [10], we used this model to extract elastic and inelastic mean free paths (MFPs) from the reflection and transmission spectra of multilayer graphene. This model can easily be modified to allow for material-specific reflectivities r and loss factors β in the hBN and graphene layers.

Fig. 3 shows toy-model transmission and reflection spectra of electrons incident on heterostacks calculated with different losses and reflectivities for graphene and hBN. For graphene, we choose $\beta = \exp(-a{\cdot}k/20)$, with wavenumber k and layer spacing a, (equivalent to $\lambda_{\text{inel}} = \frac{10}{2\pi}\lambda = 1.6\,\lambda$, with energy-dependent electron wavelength λ) to model an inelastic loss that increases with energy like seen in previous experiments [19]. The intensity loss factor β^2 is plotted in the Fig. 3 in black. The spectra are calculated for electrons incident from either side to investigate this (a)symmetry. Comparison of the micrographs of 1Gr2hBN and 2Gr1hBN in Fig. 1 shows that the predominantly hBN-like stack is both more reflective and more transmissive, i.e., has less loss. Therefore, we choose to model hBN with a doubled electron reflectivity relative to graphene, i.e., $r^2_{\text{hBN}} = 2{\cdot}r^2_{\text{Gr}}$. Additionally, with the inelastic MFP given by $\lambda_{\text{inel}} = -a/(2\ln\beta)$ (with layer spacing a), we set the inelastic MFP in hBN to twice that in graphene, i.e. $\beta_{\text{hBN}} = \sqrt{\beta_{\text{Gr}}}$. We kept the phase propagation the electron wave undergoes over a layer distance the same for both hBN and graphene, as the interlayer distance is almost the same (3.35 Å in graphene vs. 3.31 Å in hBN).

In Fig. 3 we show the resulting curves for a heterostack consisting of one layer of graphene and one (1Gr1hBN), two (1Gr2hBN), or three (1Gr3hBN) layers of hBN. All of the curves show interference minima in reflection (maxima in transmission) around 2.5 eV. These features are associated with the interlayer resonances and allow for determination of the (total) layer count. Upon reversing the order of layers, the transmission spectra stay the same, as they should. However, while the reflection spectra show the same qualitative features (related to interlayer resonances) independent of orientation, there is a quantitative difference between both orientations: The reflection in the orientation with hBN on top is consistently higher than with graphene on top, as we modelled the hBN with a higher reflectivity coefficient r. Furthermore, the features measured with graphene at the LEEM-lens side (top side) are much sharper than for the flipped configuration. The reason for that is that the electron interaction with the underlying layers is diminished by the higher $r{\cdot}\beta$ for the hBN layer (i.e. higher reflectivity at the top layer, less penetration into deeper layers).

Interestingly, the toy model also suggests that the interlayer states

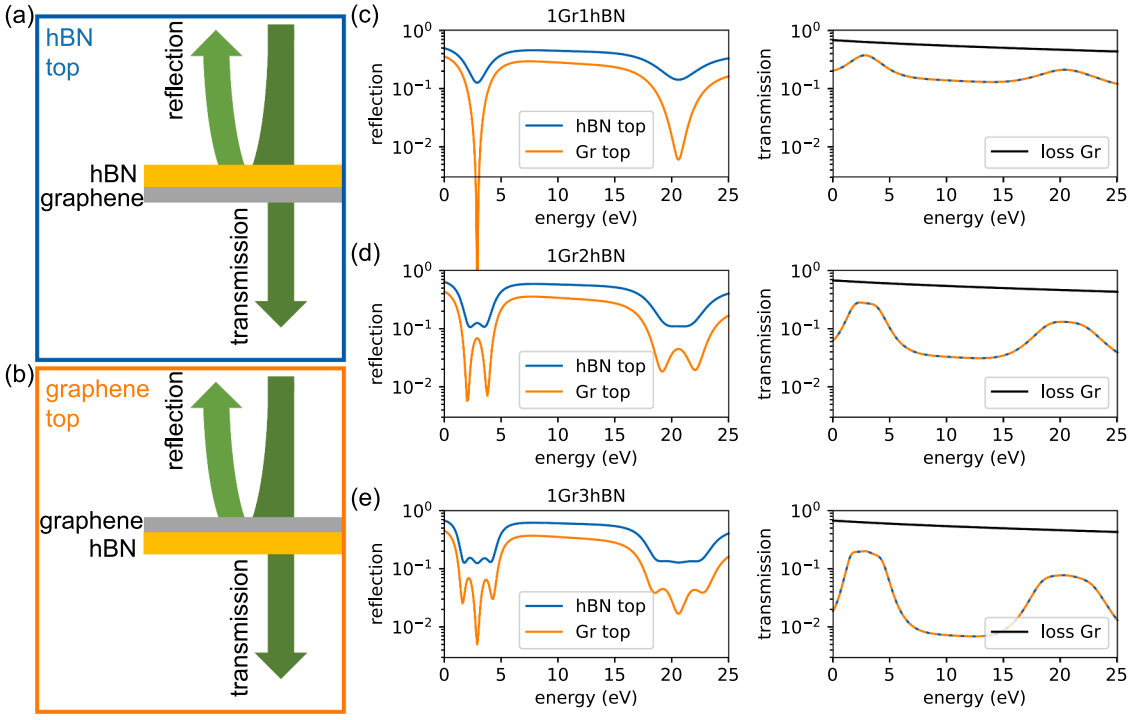

Fig. 3. Calculated toy-model reflection and transmission spectra for multiple hBN layers on top of one graphene layer (sketch in (a), blue) and the flipped stack (sketch in (b), orange). Calculation where graphene and hBN are assumed to have different inelastic reflectivity ($r^2_{\text{Gr}} = r^2_{\text{hBN}}/2 = 0.2$) and different mean free path ($\text{MFP}_{\text{hBN}} = 2{\cdot}\text{MFP}_{\text{Gr}}$). The chosen energy dependent intensity loss factor β^2 for graphene is plotted in black. The phase propagation over a unit cell is kept the same. The reflected spectrum changes upon flipping the sample, while the transmitted spectrum is invariant.

are less visible in transmission than in reflection, in accordance with the experiment (Fig. 2). However, we have not yet considered the energy widths of the respective electron guns in the toy model, which is broader for the thermal eV-TEM gun (0.75 eV) than for the cold field emitter LEEM gun (0.25 eV).

Comparing Fig. 2 to Fig. 3, we find that the experimental reflection and transmission baselines decrease more rapidly with energy than those for the toy-model calculations. This implies the inelastic MFP has a stronger energy-dependence than was assumed in our simple ansatz for β. We will see below that a larger loss also worsens the visibility of the splitting of the interference features, as it is the case for the second order interference (around 21 eV) in the experimental data.

In Fig. 4 we focus further on the relationship between the widths of the spectral features and inelastic scattering. We show reflection and transmission spectra for a 1Gr2hBN sample under various inelastic mean free paths, i.e., β-values, in the hBN, while the reflectivity of graphene and hBN is chosen this time to be the same throughout, $r^2_{\mathrm{Gr}} = r^2_{\mathrm{hBN}} = 0.2$. The inelastic loss in graphene is not varied; its inelastic loss factor β^2 vs. E is again plotted in black.

The MFPs chosen for hBN are arranged in increasing order, i.e. decreasing in loss (increasing in β) from top to bottom in Fig. 4. With decreasing loss, reflection and transmission both increase in both orientations of the sample. Accordingly, the inelastic absorption decreases. The increase in reflection is stronger for hBN on top than for graphene on top, because we vary the loss of the hBN layer.

In Fig. 4, the splitting of the interlayer band around 2.5 eV is visible in all the reflection plots. The broadening of the resonances due to inelastic processes leads to an apparent shift of the reflection minima that also depends on whether graphene or hBN is on the top. However, the splitting is (barely) visible in transmission plots for $\mathrm{MFP}_{\mathrm{hBN}} \geq 1{\cdot}\mathrm{MFP}_{\mathrm{Gr}}$ (and not at lower $\mathrm{MFP}_{\mathrm{hBN}}$). The splitting of the second-order interlayer state around 21 eV is only visible in reflection for $\mathrm{MFP}_{\mathrm{hBN}} \geq 1{\cdot}\mathrm{MFP}_{\mathrm{Gr}}$ and in transmission for $\mathrm{MFP}_{\mathrm{hBN}} \geq 2{\cdot}\mathrm{MFP}_{\mathrm{Gr}}$. We can expect interference effects to be visible when the inelastic MFP is larger or comparable to twice the interlayer spacing. All plotted cases and energies in Fig. 4, that were chosen to match the experimental data realistically, are around this length scale. However, to be detected as transmitted flux, the electron has to transverse a total of three layers, and the expectation value of the travelled path including multiple reflections is even larger. To compare

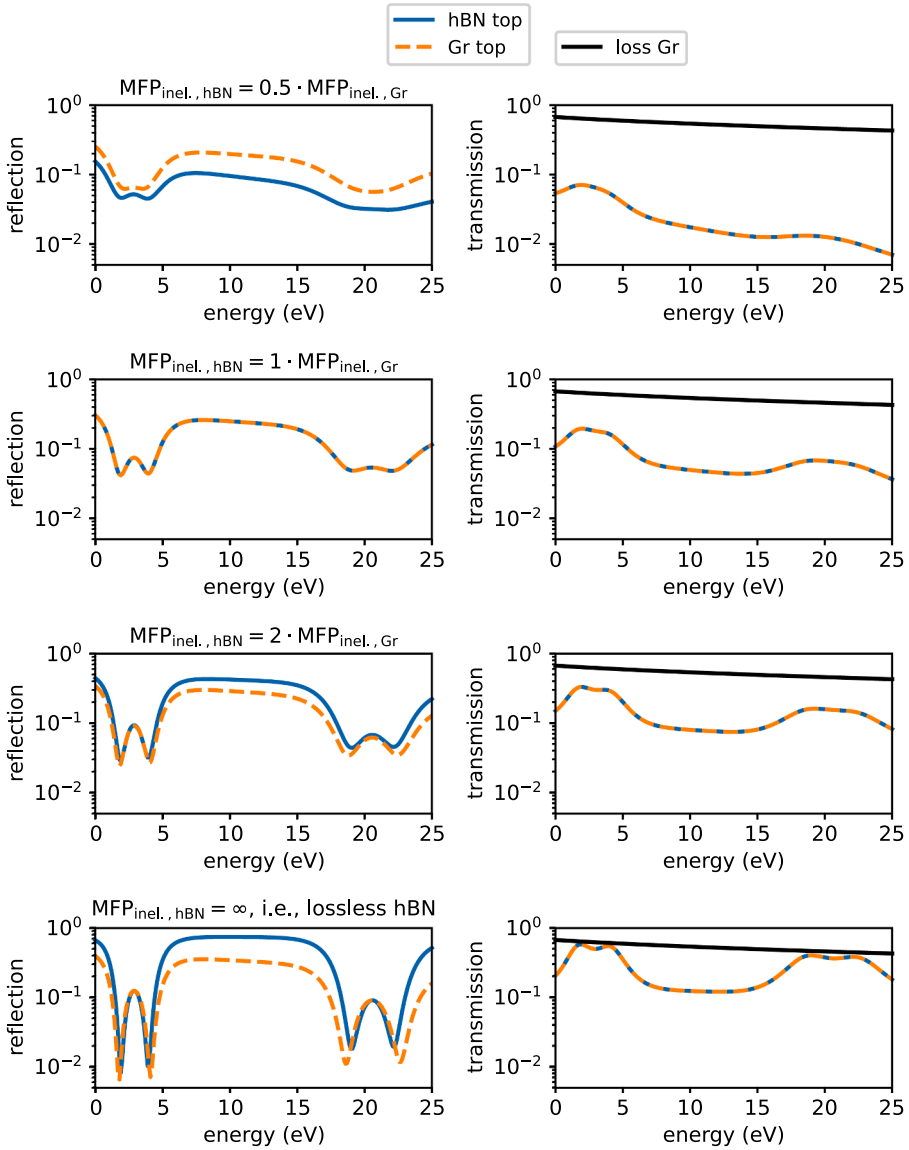

Fig. 4. Toy model reflection and transmission spectra of 1Gr2hBN for different losses in hBN, with inelastic losses in hBN decreasing top to bottom. The transmission peaks are less distinguishable at higher loss (top), i.e., lower finesse. The effect is not as strong on the reflection spectrum, though visible, especially for the incidence from the hBN side. The reflectivity of graphene and hBN are set to $r^2 = 0.2$ and the chosen energy dependent intensity loss factor β^2 for graphene is plotted in black.

to a Fabry-Pérot interferometer, where the light is reflected multiple times between mirrors with high reflectivity and very low loss, the spectral widths of peaks relative to the separation of interference orders is referred to as finesse [22]. While optical cavities typically reach a finesse of 10^3 to 10^5, the electron cavity with the reflectivity assumed in our toy model would have a finesse in the order of 1 (measured in vacuum wavelength, not in energy).

4. Spectra

After this discussion of spectral features expected due to interlayer interference, let us return to the experimental data shown in Fig. 2. When we concentrate on the spectra recorded in the original orientation first (Fig. 2c/e), some general observations are visible upon adding more layers of graphene and hBN. We will name them here, before discussing them in more detail:

1. An increased reflectivity and a decreased transmissivity baseline with an increasing number of layers.
2. At or near the resonant states, the reflectivity (transmittivity) can locally decrease (increase).
3. Splitting of the resonant states at 0–5 eV with every added layer with splitting energies slightly depending on whether graphene or hBN is added.
4. Development of the hBN-specific minima that correspond to two electron bands between 8–11 eV upon adding hBN layers [14].
5. Graphene/hBN dependent shifts of the ~20 eV band.

Observation 1) is indeed expected in a framework of inelastic processes. The transmissivity has to generally decrease with layer count, as electrons are scattered inelastically with a certain probability in each layer. With a constant inelastic mean free path (λ_{IMFP}), and ignoring multiple scattering, the flux of electrons not intercepted by inelastic scattering decreases exponentially with thickness d, as $T \propto \exp(-d/\lambda_{\mathrm{IMFP}})$. Generally, the reflectivity increases with layer count (at least far from the bands which allow the electrons to propagate into the sample), as the electrons can elastically reflect from every layer with a certain probability. The reflection minima (transmission maxima) at the interlayer states split with increasing layer count, thus turning a reflection minimum at a certain energy into a maximum upon addition of a layer. This splitting can be seen as the interference of the wavefunction of an electron that undergoes multiple reflections at the layers, as we discussed above.

Still, it is notable, that the increase in reflectivity in Fig. 2c is small for an added layer of graphene compared to 1Gr1hBN, i.e., the 2Gr1hBN curve, and comparably large for added layers of hBN, i.e., the 1Gr2hBN curve. This has led us to model hBN with a larger reflectivity, $r^2_{\mathrm{hBN}} = 2 \cdot r^2_{\mathrm{Gr}}$, in Fig. 3.

Remarkably, in the eV-TEM spectra the splitting of the interlayer state leads to a striking situation, where the transmissivity of the 1Gr2hBN stack oscillates around the transmissivity of the 1Gr1hBN stack, i.e., the transmissivity increases at 2 eV and 5 eV upon adding a layer of hBN, although the electrons have to pass three layers as opposed to two in the 1Gr1hBN case. This example shows how important it is to distinguish between elastic and inelastic MFP. In a material that is dominated by inelastic scattering, a thicker sample would always have a lower transmissivity.

As to observation 3), in the LEEM spectra in Fig. 2c, the energy resolution is sufficient for counting the total number of layers. In eV-TEM (Fig. 2e) in the same measurement configuration, the splitting is just barely visible. For one part, we relate this difference to the different impact of inelastic losses on the visibility of these splittings in reflection and transmission, as seen in Fig. 4. Furthermore, the energy dispersion of the eV-TEM electron gun is about three times that of the LEEM gun.

The transmission for 1Gr2hBN is larger than for 2Gr1hBN (both three layers total), indicating that Gr is more lossy (shorter inelastic MFP) than hBN over the full energy range. This has led us to choose a larger loss for graphene in Fig. 3.

As for Observation 4), the resonances around 8–11 eV are known from bulk hBN data and calculations, e.g., [13,14,23–25], but do not exist in graphene, nor in graphite (compare [19,26]). In the LEEM spectrum, this feature is visible for the data with only one layer of hBN and it splits in two distinguishable dips for more layers of hBN, as discussed below.

Finally, Observation 5) concerns the resonant state around 20 eV, that manifests itself in the data as a minimum in reflectivity and a maximum in transmissivity. It shifts to lower energy for more graphene-like heterostacks and to higher energy for more hBN-like heterostacks. The state is seen in both (bulk) graphene and (bulk) hBN. In our interference toy model, it is the result of the next-order interlayer resonance (as compared to the 0–5 eV split band). No layer-dependent splitting of the state is visible, however, which is attributed to increased inelastic scattering at higher energies.

5. Calculated location of states

While the interference toy model explains the interlayer states and gives an intuition for inelastic losses, it cannot capture the hBN specific band at 8–11 eV. Hence, we introduce more advanced modelling in this section. In fact, since the experimental spectra are acquired on free-standing areas, they are free of substrate effects and especially suited for comparison to (and testing of) calculations. To simulate and interpret the experiment, electron density plots and the resulting reflectivity spectra (Fig. 5 and 6) were calculated. We calculated the wavefunction for low energy electrons incident on one side of the respective heterostack. This was done for three stacks in both possible directions, i.e. for 1Gr1hBN, 1Gr2hBN, and 2Gr1hBN. We solve the Schrödinger equation by matching Bloch waves inside the material and outside the material (in vacuum) [27,28]. The reflectivity spectra (Fig. 6) are obtained from the amplitudes of the reflected wave.

The color map in each plot of Fig. 5 shows the electron density (normalized from 0 to the respective maximum), thus the absolute square of the electron wave function at a given energy. As the calculation is done in three dimensions, the electron density is projected onto the out-of-plane dimension. The horizontal axis shows the out-of-plane dimension, or z-axis, with the electrons incident from the right, and the position of each layer marked. The transmission states show up as maxima on the left side of the sample (the transmission side), and minima on the right side of the sample (the electron incidence and reflection side). The transmission states go hand in hand with characteristic localized density maxima inside of the sample, that indicate their hBN-, graphene or interlayer-like character. While the reflection spectra in Fig. 6 coincide for the two flipped orientations of a stack (as required by the Schrödinger equation for a lossless system), the projected electron densities in Fig. 5 actually differ. We will use the electron density plots to show that the measured LEEM spectra are dominated by the states closest to the surface facing the electron gun, as inelastic scattering leads to a finite probing depth in LEEM.

The calculated reflection spectra for the 1Gr1hBN, 1Gr2hBN, and 2Gr1hBN stacks are shown in Fig. 6. R(E) is the reflected intensity in the specular spot, thus directly comparable to the LEEM data. By comparison to experiment, the work function was fitted to be $\Phi = E_{\mathrm{vac.}} - E_{\mathrm{F}} \approx 4.3$ eV. We note that in these calculations no loss is applied, implying that – as long as no diffracted beams are formed – all electrons are either reflected or transmitted (in the specular spot).

We will now discuss the spectra (Fig. 6) and the electron density (Fig. 5) in conjunction, following the order of features as discussed previously for the experiments.

As in Observation 2) and 3), the lowest-energy reflectivity minimum shows an energy shift depending on the material added (dashed lines in Fig. 6). Like in our experiment, the state seen for 1Gr1hBN splits and shifts to lower energy upon the addition of a layer of hBN, whereas it

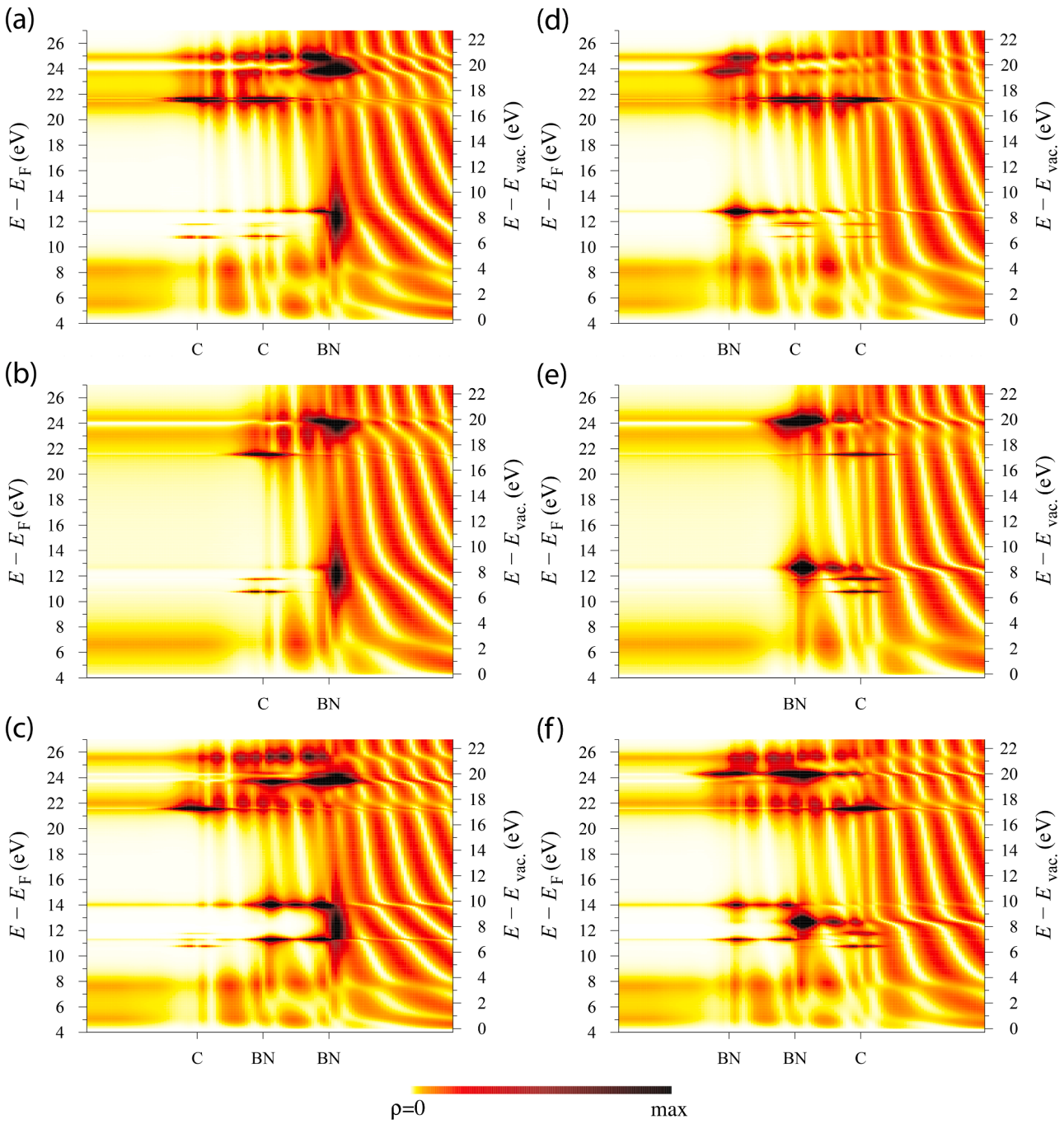

Fig. 5. Projected electron density ρ in the LEED state for the 2Gr1hBN (a,d), 1Gr1hBN (b,e) and 1Gr2hBN (c,f) stacks. The horizontal axis is the out-of-plane dimension ('z-axis') with the positions of the hBN layers (BN) and graphene layers (C) marked. The energy scale refers to the Fermi energy E_F, while the experimental spectra are given with respect to the vacuum level $E_{vac} = E_F + \Phi$, with the work function $\Phi \approx 4.3$ eV. The electron wave is incident on the sample from the right side, thus the interference of the incident and reflected wave is visible on the right of the sample, with the wavelength shortening with increasing energy. The top row shows stacks with the hBN- side facing the electron source, the bottom row shows stacks with the graphene side facing the electron source. Flipping the stack did not affect the calculated reflectivity. Note that inelastic effects are not considered here.

splits and shifts to higher energy upon the addition of a layer of graphene. The electron density of the states (Fig. 5) is centered in between the layers, as is expected for the interference state, but also has some electron density in the layer, with more in the hBN than in the graphene layer.

As in Observation 4), the hBN-specific state around $E = 9$ eV with respect to $E_{vac.}$ ($\approx E_F + 13$ eV) shows up as one minimum in the 1Gr1hBN and 2Gr1hBN spectra (dashed lines in Fig. 6), i.e., the spectra that have one hBN layer, and as two minima in the 1Gr2hBN spectrum. Other experiments [13,14,23] and calculations [13,24,29] on multilayer and bulk hBN also show two reflection minima. In all the heterostacks the electron density associated with these states is not centered in the layers, but shows up as three maxima in between the layers, resembling a $3p_z$ orbital. Independent of the orientation, the majority of the electron density is shifted towards the hBN layers, indicating that these states are hBN-specific.

The splitting of the hBN-specific state is different from the splitting of the first interference state at 3 eV. This is seen in the energy width of the

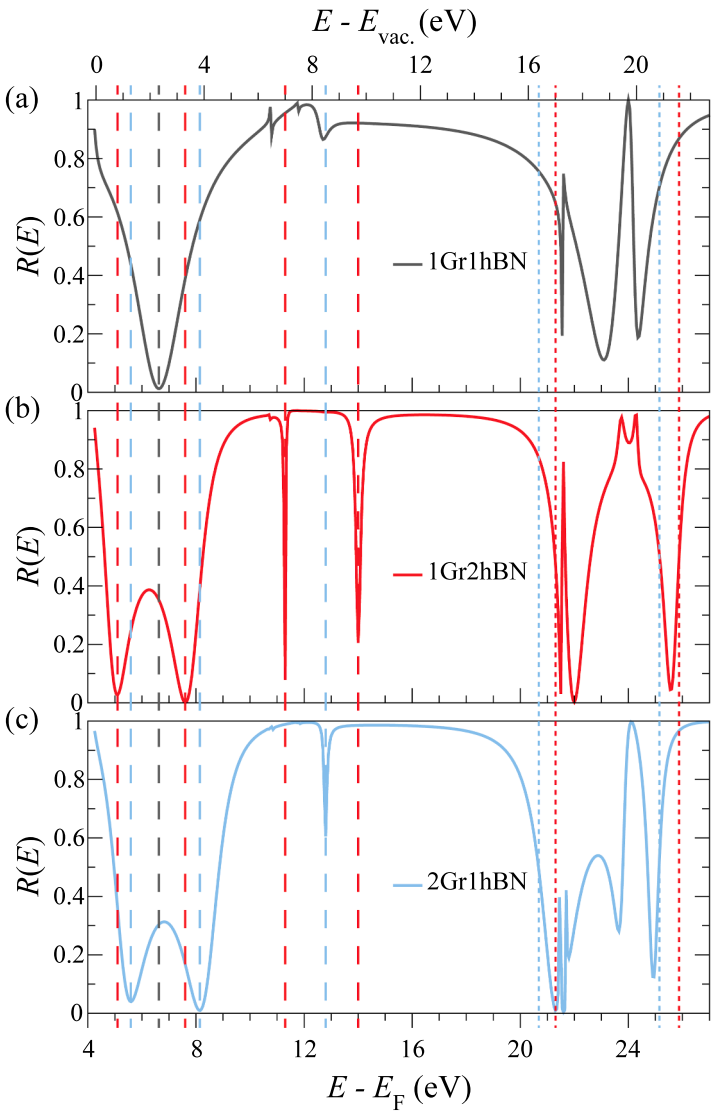

Fig. 6. Calculated reflectivity of the bilayer and the two different trilayer stacks in the specular spot without loss. The low energy reflectivity minima are marked with dashed lines in the corresponding colors to compare their energies. For the bands above 20 eV (with respect to E_F) the dotted lines indicate the energies of 50% reflectivity, as we can only resolve a general broad minimum at that high energy in experiment. The energy shifts of the low energy minima, the splitting of the ~13 eV minimum, and the general shift of the broad high energy minimum are also seen in the experiment, compare Fig. 4.

minima, which is much narrower than for the interference states, and the fact that the minima do not split further for more than two layers of hBN. For multilayer hBN, the bands are dispersive, and thus show up in the electron reflection spectra as minima, although -with their very narrow linewidth- their spectral weight is quite small.

Comparing to Observation 5), the calculations show that the broad reflection minimum at 17 to 22 eV ($\approx E_F +$ 21 to 26 eV) consists of multiple minima that shift and split depending on the composition of the heterostack. Note that the sharpest features in Fig. 6- a minimum, followed by a maximum at ~21.5 eV - is caused by the formation of the first-order diffraction beams. The range of the combined interlayer resonances is indicated in Fig. 6 by dotted lines in the respective color at 50% reflectivity. Inelastic scattering shortens the lifetime of the state and thus broadens it in energy.

The shift of this broadened band, as marked by the dotted lines at 50% reflectivity, follows the same systematics as in the experiment: it shifts to lower energy for the addition of graphene and to higher energy for the addition of hBN. However, the shift between the 2Gr1hBN and the 1Gr2hBN stack is only 0.8 eV, compared to ~3 eV in the experiment. We attribute this to inelastic scattering, which is not included in the calculation, and the resulting short inelastic mean free path (IMFP) at these higher energies. In LEEM, the probing depth is limited to the order of the IMFP (which is less than 1 layer at this energy), thus the spectrum will be dominated by the material the electrons encounter first – in this case the hBN. The LEEM spectrum at this energy thus resembles the bulk hBN spectrum (see [14]) more than the lossless calculation.

This reasoning of finite probing depth is supported by the electron density plots (Fig. 5). The broad reflection minimum is associated with states both in the graphene and the hBN at different energies. The state that is centered in the graphene layers is at lower energy ($E_F + 21.5$ eV), while the states at higher energy ($E_F +$ 23.5 to 26 eV) are dominant around the hBN layers for all heterostacks. Upon including inelastic losses, we expect to probe more of the states closer to the incidence side of the LEEM electrons, thus shift to lower energy for the incidence on the graphene side and higher energy for incidence on the hBN side.

6. Conclusion

We have shown how the low electron energy reflectivity and transmissivity spectra of a freestanding graphene-hBN heterostructure

depend on both the layer count and the stacking order of the layers. As these freestanding areas are independent of substrate influences, they are especially suited for comparison to theory. The interlayer states' splitting around 1–4 eV show that there is a direct interaction of the graphene and hBN layers, consistent with an interference toy model. Hence, contamination between both layers in the sample stacked from CVD-grown films must be minimal.

The freestanding heterostructures also allowed us to test for symmetry experimentally. Theoretically, for elastic scattering from a potential, the electron transmission and reflection coefficients are invariant under flipping the electron propagation direction. The introduction of inelastic loss in our (toy) model, allows for asymmetry in reflection, but not in transmission. Experimentally, we do find differences for both the reflection (major) and transmission (minor) under illumination from both possible sides. The differences in transmission are explained by the practical geometry, specifically the asymmetric shape of the local electric field. The toy model also explains how the visibility of the interlayer states diminishes with increasing loss, comparable to the finesse decreasing with loss in an optical cavity.

Comparison to the calculated probability density of electrons in real space shows how the LEEM spectra are mostly probing the states close to the incidence surface. Thus, the finite probing depth of LEEM – caused by inelastic electron scattering – leads to different recorded spectra upon flipping the sample. The states that are specific to graphene or hBN are located at the respective layer. The interlayer states in turn are centered in between the layers and can be seen as an interference of the electron wave function upon partial reflection from both the graphene and hBN layers. More generally, the combination of eV-TEM and LEEM can serve as a unique probe for both unoccupied states and inelastic electron processes in the general realm of (heterogeneous) van der Waals materials, provided their thickness does not exceed the inelastic scatter lengths at the energies of interest [30].

Graphene-hBN heterostacks as measured here may, in turn, serve as high-transmissivity substrates for eV-TEM investigation of layers that grow better on hBN than graphene, e.g., pentacene [31], or be used to encapsulate a sample in between. Improvements to the measurement, especially in the flipped-sample geometry, may come from additional alignment degrees of freedom of the eV-TEM gun. Adding a deflector to control the incidence angle of the eV-TEM electron beam would allow for angle-resolved transmitted-electron spectra measurements, complementary to ARRES and ARPES.

Funding

This work was supported in part by the Spanish Ministry of Science and Innovation (EEK, Projects PID2022–139230NB-I00 and PID2022–138750NB-C22) and the Dutch Research Council (PSN, NWO Vrije Programma TNW18.071).

CRediT authorship contribution statement

Peter S. Neu: Writing – review & editing, Writing – original draft, Software, Resources, Methodology, Investigation, Data curation, Conceptualization. **Eugene E. Krasovskii:** Writing – review & editing, Software, Methodology, Investigation, Conceptualization. **Rudolf M. Tromp:** Writing – review & editing, Supervision, Methodology, Investigation, Conceptualization. **Sense Jan van der Molen:** Writing – review & editing, Validation, Supervision, Resources, Project administration, Methodology, Investigation, Funding acquisition, Conceptualization.

Declaration of competing interest

The authors declare that they have no known competing financial interests or personal relationships that could have appeared to influence the work reported in this paper.

Data availability

Data will be made available on request.

References

[1] A.K. Geim, I.V. Grigorieva, Van der Waals heterostructures, Nature 499 (2013) 419–425, https://doi.org/10.1038/nature12385.
[2] A. Ramasubramaniam, D. Naveh, E. Towe, Tunable band gaps in bilayer transition-metal dichalcogenides, Phys. Rev. B - Condens. Matter Mater. Phys. 84 (2011) 1070–1075, https://doi.org/10.1103/PhysRevB.84.205325.
[3] J. Wang, F. Ma, W. Liang, M. Sun, Electrical properties and applications of graphene, hexagonal boron nitride (h-BN), and graphene/h-BN heterostructures, Mater. Today Phys. 2 (2017) 6–34, https://doi.org/10.1016/j.mtphys.2017.07.001.
[4] C.R. Dean, A.F. Young, I. Meric, C. Lee, L. Wang, S. Sorgenfrei, K. Watanabe, T. Taniguchi, P. Kim, K.L. Shepard, J. Hone, Boron nitride substrates for high-quality graphene electronics, Nat. Nanotechnol. 5 (2010) 722–726, https://doi.org/10.1038/nnano.2010.172.
[5] L. Wang, I. Meric, P.Y. Huang, Q. Gao, Y. Gao, H. Tran, T. Taniguchi, K. Watanabe, L.M. Campos, D.A. Muller, J. Guo, P. Kim, J. Hone, K.L. Shepard, C.R. Dean, One-Dimensional Electrical Contact to a Two-Dimensional Material, Science (80-.) 342 (2013) 614–617, https://doi.org/10.1126/science.1244358.
[6] L. Martini, V. Mišeikis, D. Esteban, J. Azpeitia, S. Pezzini, P. Paletti, M. W. Ochapski, D. Convertino, M.G. Hernandez, I. Jimenez, C. Coletti, Scalable High-Mobility Graphene/hBN Heterostructures, ACS Appl. Mater. Interfaces 15 (2023) 37794–37801, https://doi.org/10.1021/acsami.3c06120.
[7] Y. Cao, V. Fatemi, S. Fang, K. Watanabe, T. Taniguchi, E. Kaxiras, P. Jarillo-Herrero, Unconventional superconductivity in magic-angle graphene superlattices, Nature 556 (2018) 43–50, https://doi.org/10.1038/nature26160.
[8] R.M. Torres-Rojas, D.A. Contreras-Solorio, L. Hernández, A. Enciso, Band gap variation in bi, tri and few-layered 2D graphene/hBN heterostructures, Solid State Commun 341 (2022) 114553, https://doi.org/10.1016/j.ssc.2021.114553.
[9] J. Jung, A.M. Dasilva, A.H. Macdonald, S. Adam, Origin of band gaps in graphene on hexagonal boron nitride, Nat. Commun. 6 (2015) 1–11, https://doi.org/10.1038/ncomms7308.
[10] P.S. Neu, D. Geelen, R.M. Tromp, S.J. van der Molen, Extracting transverse electron mean free paths in graphene at low energy, Ultramicroscopy 253 (2023) 113800, https://doi.org/10.1016/j.ultramic.2023.113800.
[11] H. Hibino, H. Kageshima, F. Maeda, M. Nagase, Y. Kobayashi, H. Yamaguchi, Microscopic thickness determination of thin graphite films formed on SiC from quantized oscillation in reflectivity of low-energy electrons, Phys. Rev. B - Condens. Matter Mater. Phys. 77 (2008) 1–7, https://doi.org/10.1103/PhysRevB.77.075413.
[12] J. Jobst, J. Kautz, D. Geelen, R.M. Tromp, S.J. van der Molen, Nanoscale measurements of unoccupied band dispersion in few-layer graphene, Nat. Commun. 6 (2015) 8926, https://doi.org/10.1038/ncomms9926.
[13] H. Hibino, S. Wang, C.M. Orofeo, H. Kageshima, Growth and low-energy electron microscopy characterizations of graphene and hexagonal boron nitride, Prog. Cryst. Growth Charact. Mater. 62 (2016) 155–176, https://doi.org/10.1016/j.pcrysgrow.2016.04.008.
[14] J. Jobst, A.J.H. van der Torren, E.E. Krasovskii, J. Balgley, C.R. Dean, R.M. Tromp, S.J. van der Molen, Quantifying electronic band interactions in van der Waals materials using angle-resolved reflected-electron spectroscopy, Nat. Commun. 7 (2016) 13621, https://doi.org/10.1038/ncomms13621.
[15] Graphene Laboratories, Single layer h-BN (Boron Nitride) Film grown on Copper Foil, (2022). https://www.graphene-supermarket.com/products/single-layer-h-bn-boron-nitride-film-grown-on-copper-foil-2-x-1 (accessed May 28, 2022).
[16] Graphenea, Monolayer graphene on Cu, (2020). https://www.graphenea.com/collections/buy-graphene-films/products/monolayer-graphene-on-cu-4-inches?variant=276514394 (accessed November 7, 2023).
[17] Ted Pella Inc., PELCO® Silicon Nitride Support Films for TEM, Prod. Overv., 2011. https://www.tedpella.com/grids_html/silicon-nitride-holey.aspx (accessed November 2, 2023).
[18] X. Zhang, C. Xu, Z. Zou, Z. Wu, S. Yin, Z. Zhang, J. Liu, Y. Xia, C. Te Lin, P. Zhao, H. Wang, A scalable polymer-free method for transferring graphene onto arbitrary surfaces, Carbon N. Y. 161 (2020) 479–485, https://doi.org/10.1016/j.carbon.2020.01.111.
[19] D. Geelen, J. Jobst, E.E. Krasovskii, S.J. van der Molen, R.M. Tromp, Nonuniversal transverse electron mean free path through few-layer graphene, Phys. Rev. Lett. 123 (2019) 086802, https://doi.org/10.1103/PhysRevLett.123.086802.
[20] K. Konishi, G. Paffuti, The Schrödinger equation. Quantum Mech., Oxford University PressOxford, 2009, pp. 49–88, https://doi.org/10.1093/oso/9780199560264.003.0003.
[21] Y.V. Nazarov, Y.M. Blanter, Scattering, Quantum Transp.: Introd. to Nanoscience, Cambridge University Press, 2009, pp. 7–123.
[22] N. Ismail, C.C. Kores, D. Geskus, M. Pollnau, Fabry-Pérot resonator: spectral line shapes, generic and related Airy distributions, linewidths, finesses, and performance at low or frequency-dependent reflectivity, Opt. Express 24 (2016) 16366, https://doi.org/10.1364/OE.24.016366.
[23] P.C. Mende, Q. Gao, A. Ismach, H. Chou, M. Widom, R. Ruoff, L. Colombo, R. M. Feenstra, Characterization of hexagonal boron nitride layers on nickel surfaces by low-energy electron microscopy, Surf. Sci. 659 (2017) 31–42, https://doi.org/10.1016/j.susc.2017.02.004.

[24] L. Schué, L. Sponza, A. Plaud, H. Bensalah, K. Watanabe, T. Taniguchi, F. Ducastelle, A. Loiseau, J. Barjon, Bright Luminescence from indirect and strongly bound excitons in h-BN, Phys. Rev. Lett. 122 (2019), https://doi.org/10.1103/PhysRevLett.122.067401.
[25] C. Herrmann, P. Omelchenko, K.L. Kavanagh, Growth of h-BN on copper (110) in a LEEM, Surf. Sci. 669 (2018) 133–139, https://doi.org/10.1016/j.susc.2017.11.021.
[26] H. Hibino, H. Kageshima, F. Maeda, M. Nagase, Y. Kobayashi, Y. Kobayashi, H. Yamaguchi, Thickness determination of graphene layers formed on SiC using low-energy electron microscopy, E-Journal Surf. Sci. Nanotechnol. 6 (2008) 107–110, https://doi.org/10.1380/ejssnt.2008.107.
[27] E.E. Krasovskii, Augmented-plane-wave approach to scattering of Bloch electrons by an interface, Phys. Rev. B 70 (2004) 245322, https://doi.org/10.1103/PhysRevB.70.245322.
[28] E. Krasovskii, Ab initio theory of photoemission from graphene, Nanomaterials 11 (2021) 1212, https://doi.org/10.3390/nano11051212.
[29] Y. Malozovsky, C. Bamba, A. Stewart, L. Franklin, D. Bagayoko, Accurate ground state electronic and related properties of hexagonal boron Nitride (h-BN), J. Mod. Phys. 11 (2020) 928–943, https://doi.org/10.4236/jmp.2020.116057.
[30] P.S. Neu, M. Šiškins, E.E. Krasovskii, R.M. Tromp, S.J. van der Molen, Electron transmission and mean free path in molybdenum disulfide at electron-volt energies, Phys. Rev. B 107 (2023) 075427, https://doi.org/10.1103/PhysRevB.107.075427.
[31] A. Tebyani, Probing molecular layers with low-energy electrons. Casimir PhD series, 2024. ISBN: 978-94-6496-069-3887/3721791.